European Journal of Applied Sciences – Vol. 12, No. 06
Publication Date: December 25, 2024
DOI:10.14738/aivp.1206.17409.
Sene, M. B., Boiro M., Kouyaté, M., Diao, A., Faye, A., & Mbow, C. (2024). Study of the Charge Carrier Diffusion of a Silicon Solar Cell in the Unsteady Regime Under Multispectral Illumination: Effect of Frequency and Recombination Rate. European Journal of Applied Sciences, Vol - 12(06).824-834.

Study of the Charge Carrier Diffusion of a Silicon Solar Cell in the Unsteady Regime Under Multispectral Illumination: Effect of Frequency and Recombination Rate

Mamadou Bamba Sene
Solid State Physics and Materials Sciences Laboraty,
Faculty of Sciences and Techniques, University of Cheikh Anta Diop, Dakar, Senegal

Mountaga Boiro
Solid State Physics and Materials Sciences Laboraty,
Faculty of Sciences and Techniques, University of Cheikh Anta Diop, Dakar, Senegal

Mamadou Kouyaté
Solid State Physics and Materials Sciences Laboraty,
Faculty of Sciences and Techniques, University of Cheikh Anta Diop, Dakar, Senegal

Amadou Diao
Solid State Physics and Materials Sciences Laboraty,
Faculty of Sciences and Techniques, University of Cheikh Anta Diop, Dakar, Senegal

Alioune Faye
Fluid Mechanics and Applied Dynamics System Laboraty,
Faculty of Sciences and Techniques, University of Cheikh Anta Diop, Dakar, Senegal

CheikhMbow
Fluid Mechanics and Applied Dynamics System Laboraty,
Faculty of Sciences and Techniques, University of Cheikh Anta Diop, Dakar, Senegal

ABSTRACT

In this paper, the three-dimensional diffusion of photogenerated charge minority carriers in a polycrystalline silicon solar cell under multispectral illumination in the unsteady regime has been investigated by a numerical method; in order to optimize photocell efficiency. The influence of grain illumination frequency and recombination rate at grain boundaries on the charge carrier density and photocurrent density of a polycrystalline silicon solar cell was also investigated. From the continuity equation for minority carriers in the base, expressions for photocurrent density as a function of junction recombination rate have been derived for different values of grain size and grain boundary recombination rate.

The influence of time on the minority carrier density and on the electrical power delivered by the solar cell was presented. The photocurrent density was studied as a function of the recombination rate. The aim is to carry out a numerical resolution, making fewer simplifying assumptions to bring the study closer to reality compared with other resolution methods.

Keywords: Solar cell, recombination rate, frequency, semiconductor, charge carrier density, photocurrent.

INTRODUCTION

Energy is something that determines many other resources, such as water, education, health... The much-talked-about solar photovoltaics cover less than 1 percent of the world's energy needs.Silicon is a basic material that is widely used in the production of photovoltaic cells. The work carried out in this article is complex in resolution and important for understanding how solar cells behave under different conditions. In the dynamic frequency range, changes in frequency affect the diffusion capacity of charge carriers. Photovoltaic energy is a source of hope in the face of socio-economic and ecological constraints linked to energy, leading to the development of research into renewable energies.

With a view to contributing to research in this field, we have chosen to carry out a study highlighting the effectiveness or otherwise of the model used, based on numerical analysis as a working tool.

Theory

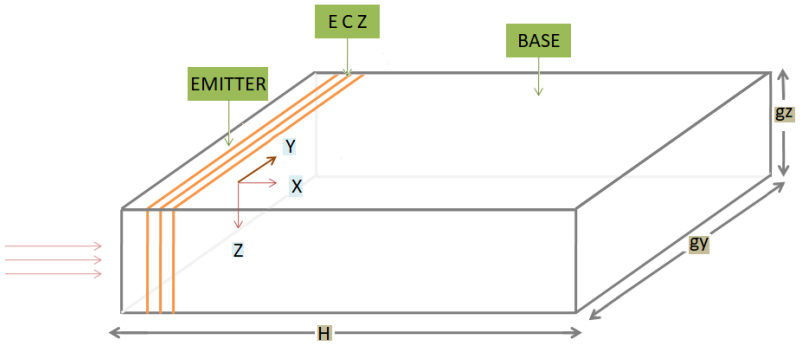

Figure 2.1

Figure 2.1 shows the geometry of the photovoltaic solar cell and the typological considerations and experimental conditions. We consider a polycrystalline silicon photopile. The contribution of the base to the current photo is greater thanthat of the transmitter [1], doping is not uniform and out of balance the recombination phenomena are accompanied by flows of carriers that participate in the establishment of permanent regimes and balance restoration [2]. The polycrystalline silicon photopile grain considered is of type $\boldsymbol{n^+/p/n^+}$of depth $\boldsymbol{H}$, length$\boldsymbol{gz}$and width $\boldsymbol{gy}$ initially in thermodynamic equilibrium.

From a moment $t = \boldsymbol{t_0}$, the front face marked $x = 0$,is subjected to polychromatic flux density radiation

$$\Phi = \sum_\lambda \phi_\lambda = \sum_\lambda \phi_{0,\lambda} \tag{2.1}$$

Since we are in the unsteady regime under multispectral illumination then we have:

$$G_n(x,t) = G_p(x,t) = \left[\sum_\lambda (1-R_\lambda).\alpha_\lambda.\phi_{0,\lambda}.e^{-\alpha_\lambda.x}\right].\mathcal{R}e\left[e^{-j..\omega.t}\right] \tag{2.2}$$

With

- $\boldsymbol{\mathcal{R}e[e^{-j..\omega.t}]}$which represents the temporal contribution of the incident luminous flux
- $\boldsymbol{\phi_{0,\lambda}}$the areal density of the incident monochromatic photon flux
- $\boldsymbol{j}$the pure imaginary complex number
- $\boldsymbol{R_\lambda}$the monochromatic reflection coefficient at the face $\mathbf{x = 0}$
- $\boldsymbol{\alpha_\lambda}$the monochromatic reflection coefficient, assumed to be isotropic

Model Equations

$$\frac{\partial \delta}{\partial t} + \vec{\nabla}.\left[-D.\left(\vec{\nabla}\delta\right)\right] = \left[\sum_\lambda (1-R_\lambda).\alpha_\lambda.\phi_{0,\lambda}.e^{-\alpha_\lambda.x}\right].\mathcal{R}e\left[e^{-j..\omega.t}\right] - \frac{\delta}{\tau} \tag{2.3}$$

This equation is completed by the following initial and boundary conditions

Initial Condition

$$\mathbf{t = t_0}, \forall \mathbf{M} \in (\boldsymbol{\Omega})\boldsymbol{\delta}(\mathbf{M}, \mathbf{t_0}) = \boldsymbol{\delta_i} \tag{2.4}$$

Boundary Conditions $(\partial\Omega)$
Surface recombination's are modeled by Robin-type conditions.

$$\forall t \geq t_0 \text{ and} \forall P \in (\partial\Omega), \left[-D.\left(\vec{\nabla}\delta\right)\right]_P.\vec{n}_l(P) = S_P.\delta(P,t) \tag{2.5}$$

With $\vec{\boldsymbol{n}}_{\boldsymbol{l}}$ $(\boldsymbol{P})$ normal to the numbered side (l) to the point **P.**

Adimensionalization of Equations and Boundary Conditions
In our case, we take the length of the base as the reference length. $\boldsymbol{H}$. We choose the lifespan of the carriers τ as the reference time and $\boldsymbol{\delta_i}$as the reference minority carrier. Assuming

$$X^* = \frac{X}{X_r} \tag{2.6}$$

The reduced size of X with its associated reference variable $\boldsymbol{X_r}$, equation (2.3) becomes, after adjustment. In the Cartesian coordinate system, this equation is written as

$$\frac{\partial \delta^*}{\partial t^*} - Fo.\left\{\frac{\partial^2 \delta^*}{\partial x^2} + \frac{\partial^2 \delta^*}{\partial y^2} + \frac{\partial^2 \delta^*}{\partial z^2}\right\} + \delta^* = N.\left[\sum_{\lambda}(1 - R_\lambda).\alpha_\lambda^*..exp(-\alpha_\lambda^*.H^*.x^*)\right].\mathcal{R}e\{exp(-j.\omega^*.t^*)\} \quad (2.7)$$

Expressions of Adimensionless Initial and Boundary Conditions

Taking into account the reference quantities, the dimensionless initial and boundary conditions are as follows

$$t^* = t_0^*, \forall M \in (\Omega)\delta^*(M, t_0) = 1 \quad (2.8)$$

$$-\left[\left(\overrightarrow{\nabla^*}\delta^*\right)\right]_P.\vec{n}_l(P) = Bi_P.\delta^*(P, t^*) \quad (2.9)$$

In equations (2.7) and (2.9) we have introduced adimensional groupings which are the control parameters of the problem defined by

$$N = \frac{\tau.\alpha_r.\phi_0}{\delta_i}; Fo = \frac{\tau.D}{H^2}; Bi_P = \frac{S_p}{H.D}$$

Fois the Fourier number and measures the extent of carrier scattering. The number $\mathbf{Bi_P}$ compares surface recombination rate and diffusion rate. **N** is the ratio between the luminous flux density at the front face and the initial carrier density. The problem we are going to solve is

$$\frac{\partial \delta^*}{\partial t^*} - Fo.\left\{\frac{\partial^2 \delta^*}{\partial x^{*2}} + \frac{\partial^2 \delta^*}{\partial z^{*2}}\right\} + \delta^* = N.\left[\sum_{\lambda}(1 - R_\lambda).\alpha_\lambda^*..exp(-\alpha_\lambda^*.H^*.x^*)\right].\mathcal{R}e\{exp(-j.\omega^*.t^*)\} \quad (2.10)$$

with

$$t^* = t_0^*, \forall M \in (\Omega)\delta^*(M, t_0) = 1 \quad (2.11)$$

$$\begin{cases} -\left[\frac{\partial \delta^*}{\partial x^*}\right]_{x^*=0} = Bi_f.\delta^*(x^* = 0, z^*, t^*) & (2.12.\text{a}) \\ -\left[\frac{\partial \delta^*}{\partial x^*}\right]_{x^*=1} = Bi_b.\delta^*(x^* = 1, z^*, t^*) & (2.12.\text{b}) \end{cases}$$

$$\begin{cases} -\left[\frac{\partial \delta^*}{\partial z^*}\right]_{z^*=0} = 0(for\ reasons\ of\ symmetry) & (2.13.\text{a}) \\ -\left[\frac{\partial \delta^*}{\partial z^*}\right]_{z^*=\frac{g_z}{2.H}} = Bi_g.\delta^*\left(x^*, z^* = \frac{g_y}{2.H}, t^*\right) & (2.13.\text{b}) \end{cases}$$

Numerical Modeling

The equation governing the transport of minority charge carriers is a parabolic partial differential equation whose solution depends strongly on the nature of the boundary and initial conditions. In general, it does not have an explicit analytical solution. The resolution method used is an approximate one. The calculation method is numerical. The first step in solving a concrete problem numerically is to reduce it to a discrete problem.

Discretization of the Physical Domain

The first step in numerical resolution is to approximate the continuous physical domain with a discrete domain made up of a set of elementary volumes called control volumes. ($\Delta \boldsymbol{\mathcal{V}_c}$)**.** We note $\boldsymbol{e, n, o, s, h\ et\ b}$the facet centers of the control volume **(see** Figure 2.2 **below).**

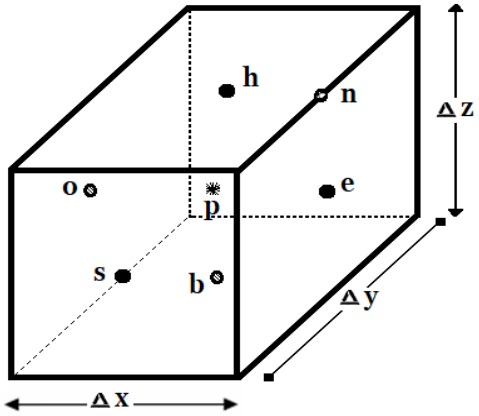

Figure 2.2: Schematic of the control volume centered at point P.

The coordinate axes are reduced to a series of regularly spaced points such that

$$\begin{cases} x_i = (i-1).\Delta x & (2.14.\text{a}) \\ y_j = (j-1).\Delta y & (2.14.\text{b}) \\ z_k = (k-1).\Delta z & (2.14.\text{c}) \end{cases}$$

With

$$\Delta x = \frac{1}{i_m - 1}, \Delta y = \frac{\left({}^{g_y}/_{2.H}\right)}{j_m - 1} et \Delta z = \frac{\left({}^{g_z}/_{2.H}\right)}{k_m - 1}$$

$\boldsymbol{i_m, j_m}$ and $\boldsymbol{k_m}$are the total number of nodes along the axes - coordinates($\boldsymbol{Ox}$) , ($\boldsymbol{Oy}$) and ($\boldsymbol{Oz}$).The discretization steps $\Delta \boldsymbol{x}.\Delta \boldsymbol{y\ and\ }\Delta \boldsymbol{z}$ are assumed to be constant, then the control volumes($\Delta \boldsymbol{\mathcal{V}_c}$)which are rectangular parallelepipeds are defined by

$$\Delta \mathcal{V}_c = \Delta x.\Delta y.\Delta z (2.15)$$

Scalar functions are then calculated at the center$\boldsymbol{P(x_i, y_j, z_k)}$of these control volumes.

Discretization of Equations and Boundary Conditions

The minority carrier equation and boundary conditions are approximated as a system of algebraic equations by integration in the generic control volume ($\Delta \boldsymbol{\mathcal{V}_c}$).

Discretization of the Minority Charge Continuity Equation

Using a centered discretization scheme to guarantee conservation of fluxes at the facets and an error of the order of the squared step, we obtain

$$\frac{\partial \delta_{i,k}}{\partial t} - Fo.\left\{\frac{\delta_{i-1,k} - 2.\delta_{i,k} + \delta_{i+1,k}}{\Delta x^2} + \frac{\delta_{i,k-1} - 2.\delta_{i,k} + \delta_{i,,k+1}}{\Delta z^2}\right\} + \delta_{i,k} = \Psi_{i,k} \quad (2.16)$$

Note that the accuracy of the carrier equation discretized in this way is of the order of space steps squared.

Discretization of Boundary Conditions

In order to obtain a system with an overall accuracy of the order of the squared discretization steps, it is therefore necessary to discretize the boundary conditions with an accuracy at least equal to that of the system (2.14). Using Taylor developments we have

$$\forall \in [1; k_m]: \begin{cases} \delta_{1,k} = \dfrac{4.\delta_{2,k} - \delta_{3,k}}{(3 + 2.\Delta x.Bi_f)} & (2.17.\text{a}) \\ \delta_{i_m,k} = \dfrac{4.\delta_{i_m-1,k} - \delta_{i_m-2,k}}{(2.\Delta x.Bi_b + 3)} & (2.17.\text{b}) \end{cases}$$

$$\forall \in [1; i_m]: \begin{cases} \delta_{i,1} = \dfrac{4.\delta_{i,2} - \delta_{i,,3}}{3} & (2.18.\text{a}) \\ \delta_{i,k_m} = \dfrac{4.\delta_{i,k_m-1} - \delta_{i,k_m-2}}{(2.\Delta x.Bi_g + 3)} & (2.18.\text{b}) \end{cases}$$

we obtain the following equation after calculation.

$$\begin{aligned} &\left(1 + \frac{\Delta t}{2}\right).\delta_{i,k} - \frac{Fo.\Delta t}{2}.\left\{\left(\frac{\delta_{i-1,k} - 2.\delta_{i,k} + \delta_{i+1,k}}{\Delta x^2} + \frac{\delta_{i,k-1} - 2.\delta_{i,k} + \delta_{i,,k+1}}{\Delta z^2}\right)\right\} \\ &= \left(1 - \frac{\Delta t}{2}\right).\tilde{\delta}_{i,k} + \frac{Fo.\Delta t}{2}.\left(\frac{\tilde{\delta}_{i-1,k} - 2.\tilde{\delta}_{i,k} + \tilde{\delta}_{i+1,k}}{\Delta x^2} + \frac{\tilde{\delta}_{i,k-1} - 2.\tilde{\delta}_{i,k} + \tilde{\delta}_{i,,k+1}}{\Delta z^2}\right) \\ &+ \frac{1}{2}.\{\Psi_{i,k} + \tilde{\Psi}_{i,k}\}.\Delta t \end{aligned} \quad (2.19)$$

Where $(\boldsymbol{\tilde{\delta}_{i,k}}, \boldsymbol{\tilde{\Psi}_{i,k}})$ and $(\boldsymbol{\delta_{i,k}}, \boldsymbol{\Psi_{i,k}})$ are the estimates of $(\boldsymbol{\delta}, \boldsymbol{\Psi})$ respectively at the times $\boldsymbol{t}$ and $\boldsymbol{t} + \Delta \boldsymbol{t}$.

RESULTS

In this section, we present and analyze results from the calculation code we developed using Fortran language version 2003. The results include: the influence of grain size, surface recombination velocities and incident radiation frequency on the distribution of minority carriers, and the influence of these parameters on the electrical characteristics.

Density of Excess Minority Charge Carriers as a Function of Base Depthx

When the photovoltaic cell is illuminated by incident light, it absorbs photons of energy equal to or greater than the gap energy of the semiconductor material making up the photovoltaic cell. Each absorbed photon creates an electron-hole pair in the base. The density of photogenerated electrons varies with the depth of the base and the intensity of illumination on the photopile. We will then study the density profile of excess minority charge carriers as a function of base depth for different values of grain boundary recombination velocity and frequency.

Study of the Effect of Junction Recombination Speed on the Density of Excess Minority Charge Carriers:

Figure 3.1 shows the profile of minority carrier density as a function of depth x for different values of recombination velocity at the junction.

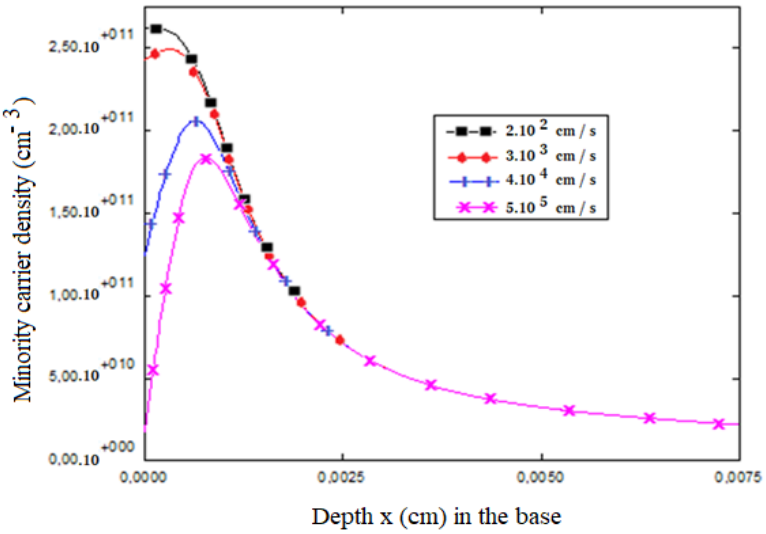

Figure 3.1: Charge carrier density as a function of depth for different values of junction recombination velocity.

Figure 3.1 shows that as the rate of recombination increases, the density of charge carriers in the base decreases. In other words, the lower the recombination rate, the higher the performance of a solar cell. Today's trend in solar cell design is to produce cells with ever-lower surface recombination rates, in order to increase efficiency [3].

In addition, the density of charge carriers in the base increases until it reaches a maximum corresponding to a depth x0 of the base. When the depth x is greater than x0, the density

decreases to the limit of the base depth (x = H). Consequently, we identify two regions on the above curve as a function of base depth:

region 1 ($x < x_0$): where the gradient of the carrier density is positive. This translates into a photocurrent-generating electron flow across the emitter-base junction;

region 2 ($x_0 < x \leq H$): where the gradient of the density of excess minority charge carriers in the base is negative. This is explained by a progressive decrease in the incident luminous flux in the depth of the base, leading to a reduction in the generation of minority charge carriers that contribute to the photocurrent. These two regions are limited to the depth **($x = x_0$)** where the density of excess minority carriers in the base is at a maximum, corresponding to a zero gradient: negative charge carriers are therefore stored, leading to a capacity of the space charge zone from the junction **(x = 0)** to the valuex_0.

Study of the Effect of Illumination Frequency on the Density of Excess Minority Charge Carriers:

Figure (3.2) shows the profile of minority carrier density as a function of depth z for different values of illumination frequency.

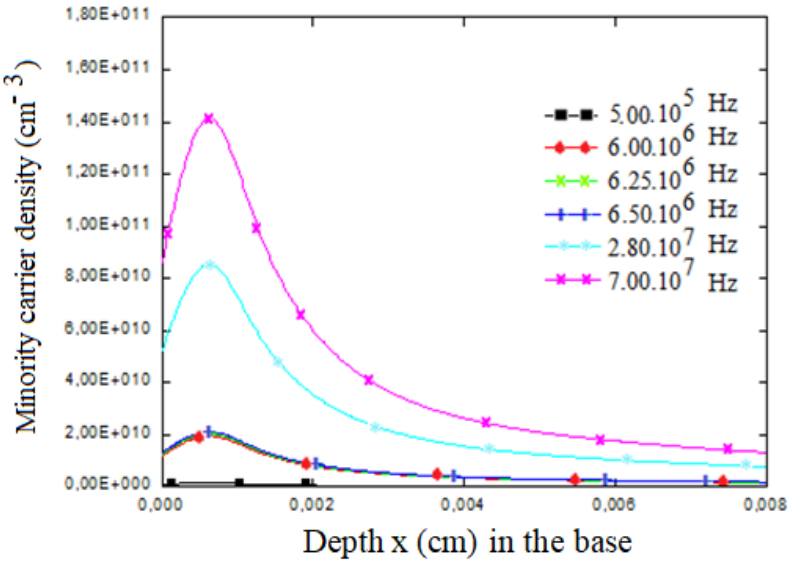

Figure 3.2: Charge carrier density as a function of base depth for different frequency values

Figure 3.2 shows that as the frequency applied to the photocell increases, so does the amplitude of the density of minority charge carriers photocrossed in the base. There's a zone where the density amplitude is at a maximum, so the gradient is zero; there's also a zone preceding the zone where the gradient is zero; in this zone the amplitude increases, so the gradient is positive; and at the end there's a zone where the amplitude decreases, so the gradient is negative.

These three zones correspond respectively to storage of minority carriers, passage of electron flow and attenuation of the incident wave.

Study of Photocurrent Density

The photocurrent is obtained from the expression.

Photocurrent Density as A Function of Recombination Rate for Different Grain Size Values:

Figure (3.3) shows the photocurrent density profile as a function of recombination speed for different grain size values.

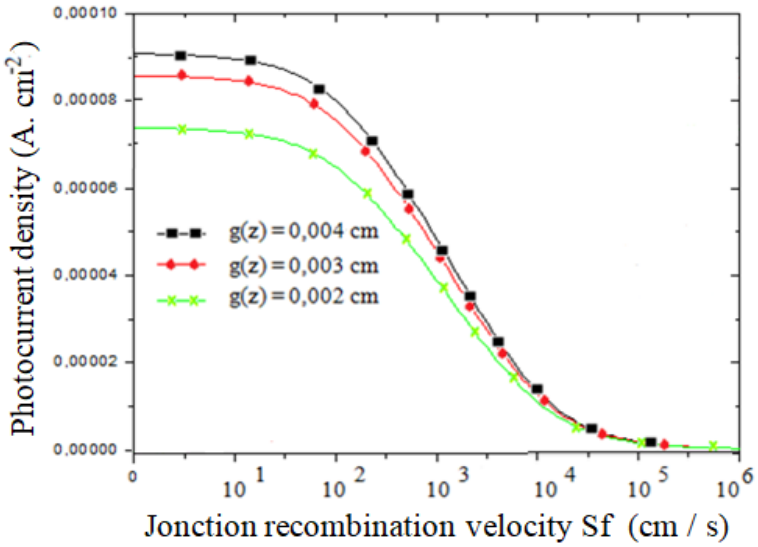

Figure 3.3: Photocurrent density as a function of recombination rate for different grain size values.

The curve shows that photocurrent density increases as a function of recombination speed. At high recombination speeds, photocurrent density tends towards a limiting value, the short-circuit current, while at low recombination speeds the current is very low, the open circuit. The variation of photocurrent density as a function of recombination speed for different values of grain size also shows that for recombination speeds below 10^2 cm/s, seed size has no influence on photovoltage, whereas for recombination speeds above 10^3 cm/s, photovoltage increases as a function of grain size [3].

Photocurrent Density as A Function of Junction Recombination Rate for Different Values of Junction Recombination Rate:

Figure (3.4) shows the photocurrent density profile as a function of the recombination rate at the junction for different values of the recombination rate at the grain boundaries.

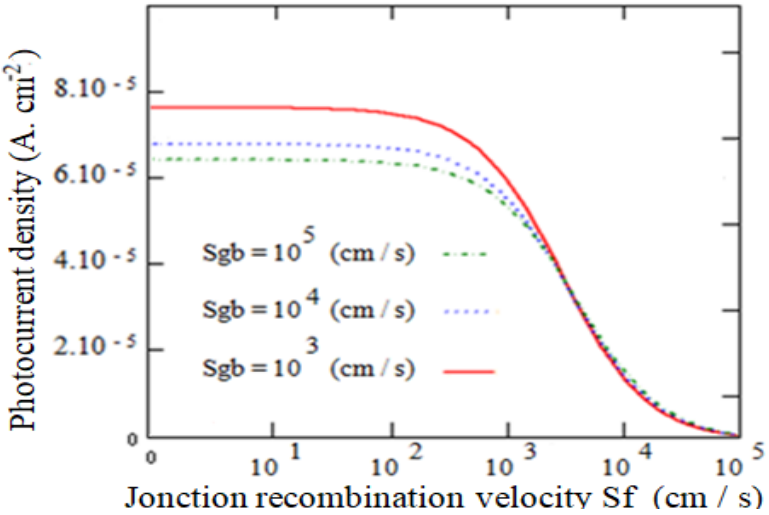

Figure 3.4: Photocurrent density as a function of junction recombination rate for different recombination rate values at grain boundaries.

Figure 3.4 also shows a range of recombination velocities from 0 to 10^2 cm/s and a range for recombination velocity values above 10^3 cm/s, where phototension is successively insensitive to recombination velocity and varies with it. Phototension is also insensitive to grain size at high recombination speeds, then increases with grain size.

Electrical Characteristics

Each photovoltaic cell or module has its own operating characteristics, represented by the non-linear characteristic curves I(V) and P(V). They present several important parameters.

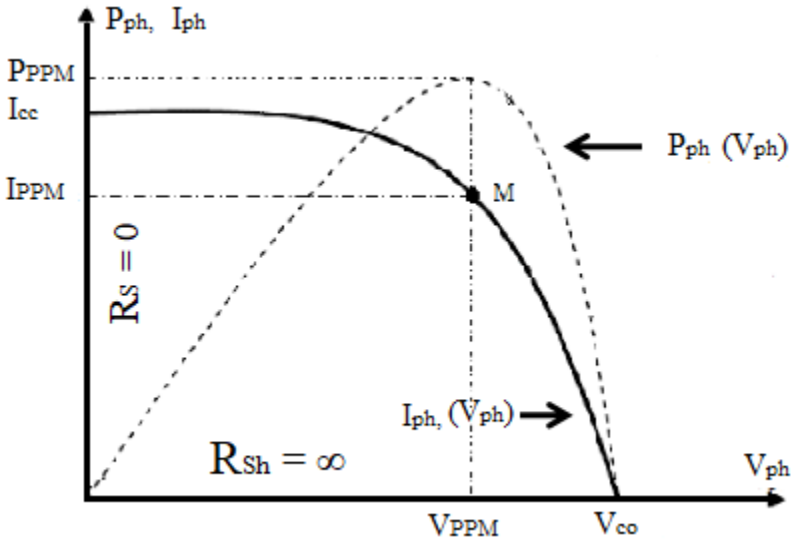

Figure 3.10: Current-voltage and power-voltage characteristics

The short-circuit current I_{CC}: is directly proportional to illumination and varies with grain size.

Voltage in open circuit V_{OC}: varies logarithmically with illumination and grain size [4].

Point of maximum power (PPM): The interesting part of the feature I(V), for the user, it's the one that generates energy. So, it won't be at the open-circuit voltage point, nor at the short-circuit point, which generate no energy, since power is the product of current and voltage P = V.I. The point of maximum power is the operating point M(V_{PPM}, I_{PPM}) for which the power dissipated in the resistive load is maximum [4].

Parameters Influencing the Operation of a Photovoltaic Cell

The frequency and speed of recombination are the focus of our study. But there are other parameters such as temperature or grain size that can modify the characteristics of a photovoltaic cell, and in particular the power delivered by the photovoltaic cell. To better understand how a photovoltaic cell works, let's trace its characteristics I(V) and P(V) for several values of illumination frequency and recombination rate.

CONCLUSION

We have just carried out a numerical three-dimensional study of the polycrystalline silicon solar cell under multispectral illumination in the unsteady regime. This study enabled us to determine the photopile's recombination parameters. In our work, we set out the equation model that corresponds to the specific case of our problem, the numerical adimensional equations and the working conditions. The results obtained for the recombination parameters are of the same order of magnitude as those published by other authors. We have studied the effect of illumination frequency and recombination rate at grain boundaries on charge carrier density. In our study, we have presented the resolution method in a concise manner. The study can be extended by determining the electrical parameters (series resistance, shunt resistance, ideality factor, form factor and photoconversion efficiency). An extension of this work can be envisaged by carrying out a transient dynamic regime study as a function of time in the presence of a magnetic field. A transient dynamic regime study could also be carried out by varying the operating point under constant illumination.

References

[1]. Zerbo. I, Zoungrana. M, SeréA.d, Ouedraogo. F, Sam. R, Zouma. B, Zougmoré. F. Revue des Energies RenouvelablesVol. 14 N°3 (2011) 517 – 532 Influence of an electromagnetic wave on a silicon photopile under static multi spectral illumination.

[2] M. B. Sene: Theoretical and numerical unsteady-state study of the three-dimensional diffusion of photogenerated minority charge carriers in a polycrystalline silicon solar cell under multispectral illumination. PhD thesis UCAD, FST 2023

[3] C. H. Tran: Improvement of a chain for the conversion of solar energy into autonomous electricity energy for application in developing countries, University of Reims Champagne Ardenne, (2019).

[4] Z. El Jouad, E.M. El-Menyawy, G. Louarn , L. Arzel , M. Morsli , M. Addou , J.C. Bernède , L. Cattin. The effect of the band structure on the Voc value of ternary planar heterojunction organic solar cells based on pentacene, boron subphthalocyanine chloride and different electron acceptors. Journal of Physics and Chemistry of Solids (IF 4), DOI: 10.1016/j.jpcs.2019.109142, 2020